Effect of composition changes on the structural relaxation of a binary mixture

W. Götze and Th. Voigtmann
Physik-Department, Technische Universität München, 85747 Garching, Germany
(Received 18 September 2002; published 19 February 2003)

Within the mode-coupling theory for idealized glass transitions, we study the evolution of structural relaxation in binary mixtures of hard spheres with size ratios δ of the two components varying between 0.5 and 1.0. We find two scenarios for the glassy dynamics. For small size disparity, the mixing yields a slight extension of the glass regime. For larger size disparity, a plasticization effect is obtained, leading to stabilization of the liquid due to mixing. For all δ, a decrease of the elastic moduli at the transition due to mixing is predicted. A stiffening of the glass structure is found as is reflected by the increase of the Debye-Waller factors at the transition points. The critical amplitudes for density fluctuations at small and intermediate wave vectors decrease upon mixing, and thus the universal formulas for the relaxation near the plateau values describe a slowing down of the dynamics upon mixing for the first step of the two-step relaxation scenario. The results explain the qualitative features of mixing effects reported by Williams and van Megen [Phys. Rev. E **64**, 041502 (2001)] for dynamical light-scattering measurements on binary mixtures of hard-sphere-like colloids with size ratio $\delta=0.6$.

DOI: 10.1103/PhysRevE.67.021502 PACS number(s): 64.70.Pf, 82.70.Dd

I. INTRODUCTION

The study of glass-transition phenomena in dense colloidal suspensions has received much attention during the past years. Such systems are well suited for a test of theories since the particles' properties can be tuned within a broad range. In particular, one can produce mixtures with particles of different sizes and observe effects of changing composition or size ratio. Recent experimental work of Williams and van Megen [1] has shown that even in the simplest of such systems, namely binary hard-sphere mixtures (HSM), interesting mixing phenomena appear for the dynamics close to the glass transition. Three effects have been reported going over from a one-component to a binary system containing up to 20% by volume of smaller spheres: (i) a shift of the glass transition to higher packing fractions, (ii) an increase in the plateau values of the correlation functions at intermediate times, connected to an increase in the glass-form factors, and (iii) a slowing down of the initial part of the relaxation towards this plateau.

In this paper, mixing effects in binary HSM are investigated in the framework of the mode-coupling theory of the idealized glass transition (MCT). The study of glass-transition phenomena in colloidal suspensions that are good realizations of one-component hard-sphere systems has revealed that MCT describes much of the experimental facts in these cases [2,3]. MCT makes general predictions for all glass-forming systems, independent of their underlying microscopic properties, be they one-component or multicomponent systems. Thus, a universal glass-transition scenario has been established, involving scaling laws and power-law variations of time scales. These properties have been found in many, not only colloidal, systems, as reviewed in Refs. [4,5]. But MCT is also able to derive detailed results depending on the specific interactions of a system. The aforementioned hard-sphere colloids are a paradigmatic example for which, among other things, the wave-vector dependence of the Debye-Waller factors in the glass state has been evaluated and compared with results from scattering experiments [3]. The quantitative study of model systems allows one to predict general, while nonuniversal, trends that arise in certain classes of glass formers. Such a project has been carried out for molecular liquids, where the known differences of reorientational relaxation for angular momentum $\ell=1$ and 2 could be explained [6,7]. The work presented here in a similar way aims to explain the general trends occurring in a mixture when changing its composition or the size disparity of its constituents. Our discussion, motivated by the cited light-scattering experiments [1], focuses on binary HSM with not too large size disparity in the species, close to the glass-transition density.

For a derivation of the MCT for mixtures, the reader is referred to Ref. [8]. The theory has already been applied to analyze computer-simulation data for a binary soft-sphere mixture [9], a binary Lennard-Jones mixture [10,11], a molecular-dynamics model of a silica melt [12], and a two-component metallic melt [13]. Also, properties of binary HSM in the limit of large size disparity [14–18] and of charged hard spheres, particularly in their low-density region [19–21], have been studied in the framework of MCT. Mixing effects in a binary HSM have been addressed recently using a standard liquid-state mode-coupling approximation, albeit for states of such low density that glassy dynamics does not occur [22,23]. MCT equations for mixtures have been derived recently within a nonlinear hydrodynamics theory [24]. The found equations are very different from the ones analyzed here, and a connection of their implications with the light-scattering data [1] was not discussed.

The paper is organized as follows. In Sec. II, we summarize the basic formulas specifying the model under study. Sections III and IV discuss our results for the fluid-glass transition diagram and the glass-form factors, respectively. We demonstrate in Sec. V that these lead to two qualitatively different scenarios for the dynamics close to the glass transition. Section VI summarizes the results.

II. DEFINITION OF THE MODEL

A. General equations of motion

A classical S-component fluid of N spherical particles shall be considered. The fluctuations of the partial number densities shall be denoted as $\varrho_\alpha(\vec{q})=\Sigma_k \exp[i\vec{q}\cdot\vec{r}_k^{(\alpha)}]/\sqrt{N}$, $\alpha=1,2,\ldots,S$, where the sum runs over all N_α particle positions $\vec{r}_k^{(\alpha)}$ belonging to the species α. From this, the partial density correlators are constructed, written as $\Phi_{\alpha\beta}(q,t)=\langle\varrho_\alpha(\vec{q})|\varrho_\beta(\vec{q},t)\rangle$. Here, $\langle A|B\rangle=\langle\delta A^*\delta B\rangle$ with $\delta A=A-\langle A\rangle$ denotes a scalar product in the space of dynamical variables. Angle brackets indicate canonical averaging for temperature T. The time evolution is generated by a Liouvillian $\mathcal{L}$: $\varrho_\alpha(\vec{q},t)=\exp[i\mathcal{L}t]\varrho_\alpha(\vec{q})$. Since the ϱ_α are spatial Fourier transforms of a real density variable in an isotropic, translational invariant system, $\Phi_{\alpha\beta}(q,t)$ is real, even in t, and it depends on the wave vector only through $q=|\vec{q}|$. An evaluation of the density correlators $\Phi_{\alpha\beta}(q,t)$ is the major aim of this paper.

The starting point of the theory is the exact reformulation of the equations of motion using the Zwanzig-Mori technique. Considering the limit of a system of colloidal particles undergoing Brownian dynamics, this equation reads

$$\boldsymbol{\tau}(q)\dot{\boldsymbol{\Phi}}(q,t)+\boldsymbol{S}(q)^{-1}\boldsymbol{\Phi}(q,t)+\int_0^t \boldsymbol{M}(q,t-t')\dot{\boldsymbol{\Phi}}(q,t')dt'=0. \tag{1a}$$

It is to be understood as a matrix equation as is indicated by the bold symbols. $\boldsymbol{S}(q)$ is the matrix of partial structure factors defined by $S_{\alpha\beta}(q)=\langle\varrho_\alpha(\vec{q})|\varrho_\beta(\vec{q})\rangle$. The short-time behavior of the correlators is given by $\boldsymbol{\Phi}(q,t)=\boldsymbol{S}(q)-\boldsymbol{\tau}(q)^{-1}|t|+\mathcal{O}(t^2)$, where $\boldsymbol{\tau}(q)$ is a symmetric positive definite matrix of relaxation times. It shall be specified in terms of short-time diffusion coefficients D_α^0 as $\tau_{\alpha\beta}(q)=1/(q^2D_\alpha^0)\delta_{\alpha\beta}$. The memory kernel $\boldsymbol{M}(q,t)$ is given by the so-called fluctuating forces, $M_{\alpha\beta}(q,t)=(k_BT)^2(x_\alpha/m_\alpha)(x_\beta/m_\beta)\langle\mathcal{Q}\mathcal{L}j_\alpha(\vec{q})|\mathcal{R}'(t)\mathcal{Q}\mathcal{L}j_\beta(\vec{q})\rangle$. Here, $\mathcal{Q}$ is the projector perpendicular to the number densities, $\varrho_\alpha(\vec{q})$, and the longitudinal parts of the number current densities $qj_\alpha(\vec{q})=\mathcal{L}\varrho_\alpha(\vec{q})$. $\mathcal{R}'(t)=\exp[i\mathcal{Q}\mathcal{L}\mathcal{Q}t]$ is the reduced evolution operator. The m_α are the masses of the species labeled by α and $x_\alpha=N_\alpha/N$ are the number concentrations.

Equation (1a) is complemented by an approximate expression for the memory kernel. The MCT approximation for this quantity follows from a straightforward generalization of the one-component case [8] and gives the polar form

$$\boldsymbol{M}(q,t)=\mathcal{F}[\boldsymbol{\Phi}(t),\boldsymbol{\Phi}(t)](q) \tag{1b}$$

of a symmetric bilinear form of the density correlators

$$\mathcal{F}_{\alpha\beta}[\boldsymbol{\Phi}^{(1)},\boldsymbol{\Phi}^{(2)}](q)=\frac{1}{2q^2}\frac{\varrho}{x_\alpha x_\beta}\sum_{\alpha'\beta'\alpha''\beta''}\sum_{\vec{k}} V_{\alpha\alpha'\alpha''}(\vec{q},\vec{k},\vec{p})\times\Phi^{(1)}_{\alpha'\beta'}(k)\Phi^{(2)}_{\alpha''\beta''}(p)V_{\beta\beta'\beta''}(\vec{q},\vec{k},\vec{p}). \tag{1c}$$

Here, ρ is the total number density, $\vec{p}=\vec{q}-\vec{k}$, and $V_{\alpha\beta\gamma}(\vec{q},\vec{k},\vec{p})$ are vertices quantifying the coupling of a force fluctuation of wave vector $\vec{q}$ to density-fluctuation pairs with wave vectors $\vec{k}$ and $\vec{p}$, respectively. The vertices are given by the equilibrium structure of the system in terms of the Ornstein-Zernike direct correlation function $c_{\alpha\beta}(q)$ and static three-particle correlations. The latter shall be expressed in terms of the $S_{\alpha\beta}(q)$ using the convolution approximation. One thus arrives at

$$V_{\alpha\alpha'\alpha''}(\vec{q},\vec{k},\vec{p})=(\vec{q}\vec{k}/q)c_{\alpha\alpha'}(k)\delta_{\alpha\alpha''}+(\vec{q}\vec{p}/q)c_{\alpha\alpha''}(p)\delta_{\alpha\alpha'}. \tag{1d}$$

A few remarks to these equations might be in order. The solution to Eqs. (1) exists for all $t\geqslant 0$, and it is uniquely determined by the initial conditions. For a system with colloidal short-time dynamics, the correlation functions $\boldsymbol{\Phi}(q,t)$ are completely monotonic functions [25]. This property is preserved by the specified MCT approximation. In detail, it implies the following. The matrices $\boldsymbol{\Phi}(q,t)$ are positive definite, written as $\boldsymbol{\Phi}(q,t)\geqslant 0$, for all times t and at all q; and for the time derivatives, there holds $(-1)^l\partial_t^l\boldsymbol{\Phi}(q,t)\geqslant 0$ for all $l=1,2,\ldots$. Furthermore, the solution depends smoothly on $S_{\alpha\beta}(q)$, $\tau_{\alpha\beta}(q)$, and $V_{\alpha\beta\gamma}(\vec{q},\vec{k},\vec{p})$ for any fixed finite time interval. At $t\to\infty$, the bifurcations in the long-time limit $\boldsymbol{F}(q)=\lim_{t\to\infty}\boldsymbol{\Phi}(q,t)$ may occur at critical points called glass-transition singularities. The $F_{\alpha\beta}(q)$ are called the glass form factors and they are solutions of the equation

$$\boldsymbol{F}(q)=\boldsymbol{S}(q)-\{\boldsymbol{S}(q)^{-1}+\mathcal{F}[\boldsymbol{F},\boldsymbol{F}](q)\}^{-1}. \tag{2a}$$

In particular, the correct $\boldsymbol{F}(q)$ can be determined through an iteration scheme, $\boldsymbol{F}^{(n)}(q)=\boldsymbol{S}(q)-\{\boldsymbol{S}(q)^{-1}+\mathcal{F}[\boldsymbol{F}^{(n-1)},\boldsymbol{F}^{(n-1)}](q)\}^{-1}$, $n=1,2,\ldots$, with starting point $\boldsymbol{F}^{(0)}(q)=\boldsymbol{S}(q)$. The sequence $\boldsymbol{F}^{(n)}(q)$ converges monotonically towards $\boldsymbol{F}(q)$. For sufficiently small vertices, one has the liquid solution $\boldsymbol{F}(q)=\boldsymbol{0}$, while the glass is characterized by $\boldsymbol{F}(q)\neq\boldsymbol{0}$. Solutions corresponding to critical points shall be denoted by a superscript c. To understand the bifurcation scenario, one needs to discuss the critical eigenvector of the linearization of Eq. (2a), $\boldsymbol{H}(q)$, given by

$$\boldsymbol{H}(q)-2[\boldsymbol{S}^c(q)-\boldsymbol{F}^c(q)]\mathcal{F}^c[\boldsymbol{F}^c,\boldsymbol{H}](q)[\boldsymbol{S}^c(q)-\boldsymbol{F}^c(q)]=\boldsymbol{0}. \tag{2b}$$

This eigenvector is nondegenerate, which implies that all MCT bifurcations belong to the type A_ℓ, $\ell=2,3,\ldots$, introduced by Arnol'd [26]. Also, one can choose $\boldsymbol{H}(q)>0$. All of the preceding remarks apply to the general case of matrix-valued MCT equations; they are not affected by the precise form of the vertices entering Eq. (1c). Proofs of the cited mathematical properties of Eqs. (1) and (2) can be found in Ref. [27]. In this paper only the simplest bifurcations, i.e., those of type A_2 are discussed, where a jump occurs in $\boldsymbol{F}(q)$ from $\boldsymbol{0}$ to the critical value $\boldsymbol{F}^c(q)>0$.

There is an important implication of the cited general results that can be substantiated in complete analogy to the one

obtained for one-component systems [28,29]. There exists a time scale t_0 such that one can express the solution of Eq. (1) for $t \gg t_0$ in the form

$$\mathbf{\Phi}(q,t) = \mathbf{S}^{1/2}(q)\,\boldsymbol{\phi}(q,\tilde{t})\,\mathbf{S}^{1/2}(q), \tag{3a}$$

where $\tilde{t} = t/t_0$. The time scale t_0 depends smoothly on $S_{\alpha\beta}(q)$, $\tau_{\alpha\beta}(q)$, and $V_{\alpha\beta\gamma}(\vec{q},\vec{k},\vec{p})$. The sensitive dependence of $\mathbf{\Phi}$ on the control parameters is described by the completely monotonic function $\boldsymbol{\phi}(q,\tilde{t})$. The latter is determined, up to some arbitrary time scale t_*, through the equation

$$\boldsymbol{\phi}(q,t) = \mathbf{m}(q,t) - \frac{d}{dt}\int_0^t \mathbf{m}(q,t-t')\,\boldsymbol{\phi}(q,t')\,dt', \tag{3b}$$

obeying the initial condition

$$\lim_{t\to 0} (t/t_*)^{1/3}\,\boldsymbol{\phi}(q,t) = \mathbf{1}. \tag{3c}$$

Here the kernel $\mathbf{m}(q,t)$ is given by the mode-coupling functional [Eq. (1c)] as

$$\mathbf{m}(q,t) = \mathbf{S}^{1/2}(q) \times \mathcal{F}[\mathbf{S}^{1/2}\boldsymbol{\phi}(t)\mathbf{S}^{1/2}, \mathbf{S}^{1/2}\boldsymbol{\phi}(t)\mathbf{S}^{1/2}](q)\,\mathbf{S}^{1/2}(q). \tag{3d}$$

This means that $\boldsymbol{\phi}(q,\tilde{t})$ is determined by the quantities entering $\mathcal{F}$ only, i.e., by the parameters specifying the equilibrium structure. In this manner, MCT justifies the concept of structural relaxation as opposed to, e.g., transient relaxation. The latter, be it Brownian or Newtonian, merely enters the scale t_0. In particular, this implies that details of $\tau_{\alpha\beta}(q)$ do not affect the structural relaxation apart from influencing t_0.

Let us also note the formulas for the longitudinal and transversal elastic moduli of the mixture. They are given through Green-Kubo relations involving the total mass currents [30,31]. One defines the projector $\mathcal{Q}_{\mathrm{HD}}$ as projecting out $\varrho_\alpha(\vec{q})$ and the longitudinal mass current, $J(\vec{q}) = \Sigma_\alpha m_\alpha j_\alpha(\vec{q})$ together with the corresponding reduced resolvent $\mathcal{R}'_{\mathrm{HD}}(z)$. The latter is the Laplace transform for frequency z of the corresponding evolution operator $\mathcal{R}'_{\mathrm{HD}}(t) = \exp[i\mathcal{Q}_{\mathrm{HD}}\mathcal{L}\mathcal{Q}_{\mathrm{HD}}t]$. For the longitudinal viscosity, this yields [30]

$$\eta^L = \lim_{z\to 0}\lim_{q\to 0} \frac{\varrho}{k_B T}\,\frac{1}{q^2}\,\langle \mathcal{Q}_{\mathrm{HD}}\mathcal{L}J(\vec{q}) | \mathcal{R}'_{\mathrm{HD}}(z)\,\mathcal{Q}_{\mathrm{HD}}\mathcal{L}J(\vec{q})\rangle. \tag{4}$$

At the bifurcation singularity, a nontrivial long-time limit $\mathbf{F}^c(q)$ implies a pole at zero frequency, $\mathbf{\Phi}^c(q,z) \sim -\mathbf{F}^c(q)/z$. According to this, the longitudinal modulus shows a discontinuity δM_L^c at the glass transition. Rewriting Eq. (4) in terms of the MCT projector $\mathcal{Q}$, one gets

$$\delta M_L^c = (\varrho k_B T)\lim_{q\to 0}\sum_{\alpha\beta} x_\alpha \mathcal{F}^c_{\alpha\beta}[\mathbf{F}^c,\mathbf{F}^c](q)\,x_\beta. \tag{5}$$

The glass, different from the liquid, is characterized by a finite shear modulus. A formula similar to Eq. (5) is obtained for the shear modulus M_T^c at the glass transition,

$$M_T^c = (\varrho k_B T)\lim_{q\to 0}\sum_{\alpha\beta} x_\alpha \mathcal{F}^{T,c}_{\alpha\beta}[\mathbf{F}^c,\mathbf{F}^c](q)\,x_\beta. \tag{6}$$

Here, the MCT expression for the transverse fluctuating-force kernel $\mathcal{F}^T(q)$ is obtained from $\mathcal{F}(q)$ by replacing in Eq. (1c) the vertices by

$$\mathcal{V}^T_{\alpha\alpha'\alpha''}(\vec{q},\vec{k},\vec{p}) = (\vec{q}^T\vec{k}/q)\,c_{\alpha\alpha'}(k)\,\delta_{\alpha\alpha''} + (\vec{q}^T\vec{p}/q)\,c_{\alpha\alpha''}(p)\,\delta_{\alpha\alpha'}. \tag{7}$$

In this formula, $\vec{q}^T$ is a vector of length q perpendicular to $\vec{q}$.

B. The binary hard-sphere mixture

The general theory shall be applied to binary hard-sphere mixtures (HSM), consisting of large (A) and small (B) particles. If d_α, $\alpha = A,B$ denote the particle diameters, the packing fractions of the species read $\varphi_\alpha = (\pi/6)(x_\alpha\varrho)d_\alpha^3$, and the total packing fraction is given by $\varphi = \varphi_A + \varphi_B$. The thermodynamic state is characterized by three control parameters. Let us choose them to be the total packing fraction φ, the size ratio $\delta = d_B/d_A \leqslant 1$, and the packing contribution of the smaller species $\hat{x}_B = \varphi_B/\varphi$. Whenever composition changes are considered in the following, a variation of $\hat{x}_B$ for fixed φ and δ is to be understood. This in turn implies the number concentration of the small particles to vary as

$$x_B = \frac{\hat{x}_B/\delta^3}{1 + \hat{x}_B(1/\delta^3 - 1)}. \tag{8}$$

The procedure is somewhat in between a true addition, which would increase both total density and total packing fraction, and a replacement of a certain amount of large spheres by the same amount of smaller ones, which would reduce the total packing fraction. For sufficiently small δ, there appears a percolation threshold for the motion of the small particles in the glass formed by the large ones. This transition and its precursor phenomena shall not be considered in this paper.

Static structure input for our model is taken from the Percus-Yevick (PY) approximation [32,33]. More accurate solutions of the Ornstein-Zernike integral equations for hard-sphere mixtures are available. Yet, one knows from the one-component MCT that improvements aiming at, for example, thermodynamic consistency have little influence on the glassy dynamics. Unfortunately, the quality of the PY approximation at the desired high packing fractions is unknown. It is known that large errors of the structure factor can occur if one goes over to large values of $1/\delta$ [34], but this case is excluded from our discussion.

With the structure factor and the direct correlation functions given, the vertices in Eqs. (1d) and (7) are well-defined functions of the wave vectors and matrix indices. Hence, also

the mode-coupling functional $\mathcal{F}$ in Eq. (1c) is defined as a triple integral over the components of $\vec{k}$; and the same holds for the functional $\mathcal{F}^T$. After introduction of bipolar coordinates and using rotational symmetry, the $\vec{k}$ integrals are transformed to double integrals over $k=|\vec{k}|$ and $p=|\vec{q}-\vec{k}|$. After performing the $\vec{q}\to 0$ limit in the functionals, the zero-wave-vector limits entering Eqs. (5) and (6) are reduced to one-dimensional integrals over k. As a next step, the wave vectors are reduced to points on a grid of M values. The grid is chosen as $qd_A=q_0+\hat{q}\Delta q$, with $q_0=0.2$, $\Delta q=0.4$, and $\hat{q}=0,1,\ldots,M-1$, unless otherwise stated. The integrals are replaced by Riemann sums. The resulting formulas are the same as explained explicitly before for the one-component systems [35], but additional sums over matrix indices occur. As a result, the cited equations refer to ones for sets of M matrix correlators, where q serves as a label for the correlators. To complete the specification of the equations, the short-time diffusion constants are taken according to the Stokes' law, $D_\alpha^0=C/d_\alpha$. The unit of time is chosen so that $C=0.01$.

For the simple hard-sphere system, it was found that a choice of $M=100$ is sufficient to avoid cutoff and discretization effects for the results [35]. Our work was done mostly with $M=200$, implying a cutoff wave vector $q^*d_A=79.8$. This enables us to handle size ratios of $\delta\geqslant 0.5$ with the accuracy used earlier for the simple system. Thus, Eqs. (1a)–(1c) are 600 coupled integro-differential equations for 600 correlators, and Eq. (2a) formulate 600 implicit equations for the 600-glass form factors. The latter equations are solved by the iteration mentioned above. Thereby, one gets the form factors as discussed in Sec. IV. Shifting the value for the packing fraction φ, one identifies the glass-transition points. The linear equation for the nondegenerate eigenvector $\boldsymbol{H}(q)$, [Eq. (2b)], is solved by a standard routine. This eigenvector is used to calculate the asymptotic solutions discussed in Sec. V B. The critical glass form factors are substituted into Eqs. (5) and (6) so that the contributions to the moduli discussed in Sec. III can be calculated.

The closed set of Eqs. (1a)–(1c) as well as Eqs.(3a)–(3d) for the time dependence of the correlators are solved by a method adapted to this special kind of Volterra problem. The solutions of Eqs. (1) yield the correlators to be compared with the cited light-scattering data. The solutions of Eq. (3b) are used in Sec. V B to separate structural relaxation from the transient dynamics. To proceed, one introduces a grid on the time axis of equal step size h consisting of N points. The time derivatives in Eqs. (1a) and (3b) are replaced by difference relations and the convolution integrals by Riemann sums. One gets a recursion relation determining the solutions for time $t_{n+1}=h(n+1)$ from the values t_l, $l\leqslant n$. The initial values are taken from the short-time asymptote, given by $\boldsymbol{\Phi}(q,t)-\boldsymbol{S}(q)\sim-\boldsymbol{\tau}(q)^{-1}t$ or Eq. (3c), respectively. Because of the scale invariance of the equations of structural relaxation, the value of t_* does not matter. One has to make sure that the results obtained for $0<t<t_N$ remain stable within the desired accuracy upon doubling h or halving N. Then one carries out a decimation by setting $h\mapsto 2h$. Thereby, one solves the equations up to $2t_N$. This procedure is repeated until the correlators reach their long-time asymptote. Details are explained, e.g., in Ref. [36]. Typically, the figures in this paper have been calculated with $h=10^{-6}$ and $N=256$. Let us point out that Eqs. (1)–(7) are completely analogous to the ones discussed repeatedly in the previous studies of one-component systems. Also the numerical methods applied for the solution are the ones used earlier for the simple case. The additional complication here is the handling of matrices; but this is straightforward though numerically more demanding.

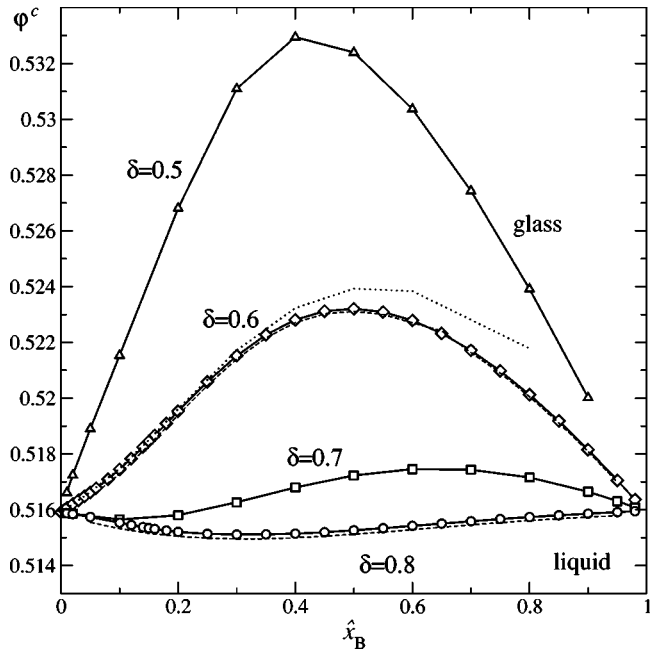

FIG. 1. Liquid-glass transition diagram of a binary hard-sphere mixture (HSM) for size ratios $\delta=0.5$ (triangles), $\delta=0.6$ (diamonds), $\delta=0.7$ (squares), and $\delta=0.8$ (circles), plotted as critical total packing fraction φ^c versus packing contribution of the smaller species, $\hat{x}_B=\varphi_B/\varphi$. Full lines are guides to the eyes. The dashed lines indicate results obtained from tripling the number M of grid points from $M=200$ to $M=600$, and the dotted line for $\delta=0.6$ shows results obtained using $M=100$; see text for details.

III. TRANSITION DIAGRAM

Cuts through the liquid-glass transition surface in the three-dimensional control-parameter space for the binary HSM are depicted in Fig. 1. To assure that the results do not seriously depend on the discretization used, we show as well the glass-transition points calculated for $\delta=0.6$ and 0.8 from the model with $M=600$, $\Delta q=0.4/3$, $q_0=0.2/3$. In addition, for $\delta=0.6$ the dotted line exhibits the result calculated with cutoff $q^*d_A=39.8$ and $M=100$, which are the discretization parameters used in Ref. [35]. One infers that for $\hat{x}_B\lesssim 0.3$, this discretization would be sufficient to produce reasonable results.

For fixed size ratio $\delta\lesssim 0.65$, the critical packing fraction first increases upon increasing $\hat{x}_B$. Since $\hat{x}_B=0$ and $\hat{x}_B=1$ both represent monodisperse hard-sphere systems, one gets $\varphi^c(\hat{x}_B=0)=\varphi^c(\hat{x}_B=1)$. Thus, the liquid-glass transition

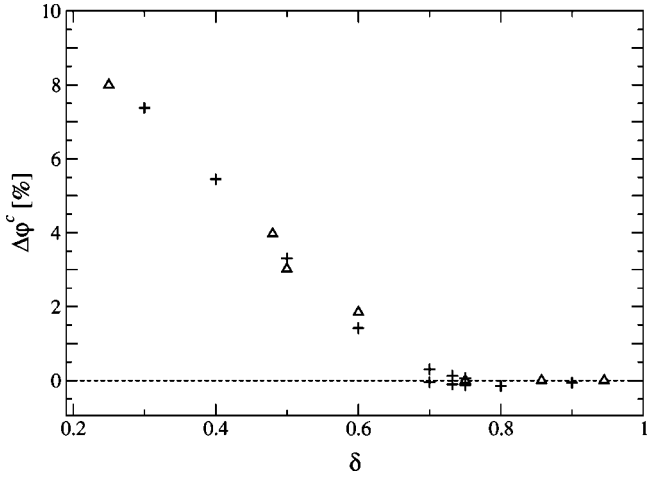

FIG. 2. Maximum relative increase and decrease of the critical packing fraction $\Delta\varphi^c(\delta)$, according to Eq. (9), as a function of the size ratio δ (crosses), together with experimental data for random loose packing (triangles, reproduced from Ref. [41], cf. text). For the MCT critical packing fraction values, two symbols are noted for those δ where a maximum and a minimum different from the $\delta=1$ value could be identified.

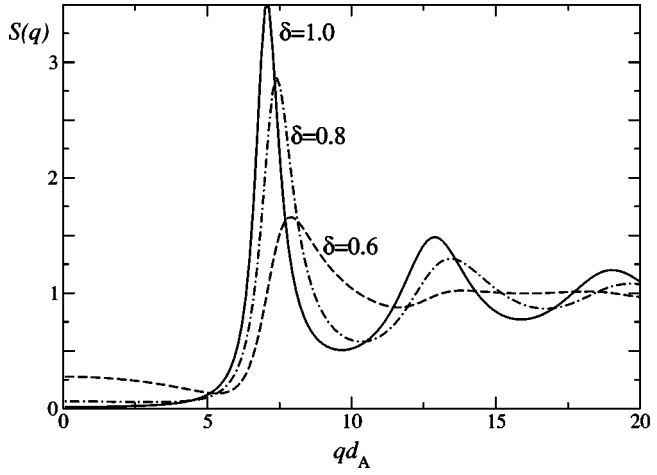

FIG. 3. Total structure factor $S(q)=\Sigma_{\alpha\beta}S_{\alpha\beta}(q)$, calculated in the Percus-Yevick approximation for binary mixtures with $\varphi=0.515$, $\hat{x}_B=0.2$ and three values of δ.

lines for $\delta\lesssim 0.65$ exhibit a maximum at some intermediate values of $\hat{x}_B$. It is well understood that big particles moving in a liquid of much smaller ones experience an effective attraction [37] that is of purely entropic origin. Such a short-ranged attraction leads to a stabilization of the liquid phase, as was explained earlier [38–40]. Our result is a direct analogon of this depletion-attraction effect. Similarly, from the discussion of polymer melts it is known that the introduction of smaller components into the system typically decreases the viscosity, i.e., drives the system further into the liquid phase; an effect sometimes called ''plasticizing.'' Therefore, the effect found here is an entropically induced plasticization effect.

For less-disparate-sized mixtures, the theory predicts an inversion of the effect described above. An example is shown in Fig. 1 for $\delta=0.8$, where a decrease of φ^c with increasing $\hat{x}_B$ up to some minimum point is observed. This is in accordance with similar MCT results for a binary soft-sphere mixture [9]. It means that the introduction of disorder due to a small polydispersity of the particles stabilizes the glass state. The transition diagram is not symmetric with respect to $\hat{x}_B\rightarrow(1-\hat{x}_B)$; our theory predicts for $0.65\lesssim\delta\lesssim 0.8$ ''*S*''-shaped transition lines.

To get another view on the transition diagram, let us define the relative change of φ^c with respect to the one-component case as

$$\Delta\varphi^c(\delta)=[\varphi^c(\delta,x_B^{\pm})-\varphi_0^c]/\varphi_0^c. \tag{9}$$

Here, $x_B^{\pm}$ are the points at which a maximum or a minimum occurs in $\varphi^c(x_B)$ for fixed δ; $\varphi_0^c\approx 0.5159$ is the critical packing fraction of the one-component system. The resulting values are plotted in Fig. 2 together with the data taken from Ref. [41]. There results for $\Delta\varphi(\delta)$ of several experiments for random loose sphere packings in two-component steel-ball mixtures have been presented. These are operationally defined as the random packing fractions obtained when pouring spheres into a container without subsequent densification through shaking. One observes that both $\Delta\varphi^c(\delta)$ and the data follow the same trend. Note that we get negative values for $0.65\lesssim\delta<1$. In Ref. [41], no such effect is discussed, but it is reported that there seems to be no observable change in the data. There is no precise theoretical definition of the concept of random loose packing. Nevertheless, the reported values can be taken as a quantization of a mixing effect, i.e., of modifications of the random cage structure. The fact that the variation in $\Delta\varphi^c$ with δ agrees with these experimental findings supports the conclusion that MCT is able to capture the change in the average cage structure induced by the presence of the second component.

The results from above suggest that the change of the glass-transition point with composition can be understood by looking at the geometrical structure of the system. This information is reflected by the static structure factors that comprise the relevant input for the MCT vertex in Eq. (1d). In particular, it is understood that the q-vector region around the first sharp peak in $S(q)$ is important for explaining the MCT glass transition. Figure 3 shows this region for the total structure factor $S(q)=\Sigma_{\alpha\beta}S_{\alpha\beta}(q)$ at fixed packing fraction $\varphi=0.515$, composition $\hat{x}_B=0.2$, and different δ. One notices two trends caused by decreasing δ, viz., a decrease in peak height and an increase in its large-q wing. The interplay between these two trends is responsible for the shift in φ^c. At larger δ, the increase in the wing is dominant and stabilizes the glass, i.e., it reduces φ^c with respect to the one-component system. But at $\delta\lesssim 0.65$, the reduction in peak height, equivalent to a weakening of the intermediate-range order, overwhelms this trend. This effect stabilizes the liquid, i.e., increases φ^c. In all cases, the peak position shifts to higher q, indicating that, on and average, particles are closer together in the mixture than in the one-component system; an effect typical for the introduction of effective attractive interactions [40].

Another way of looking at the local structure of the HSM

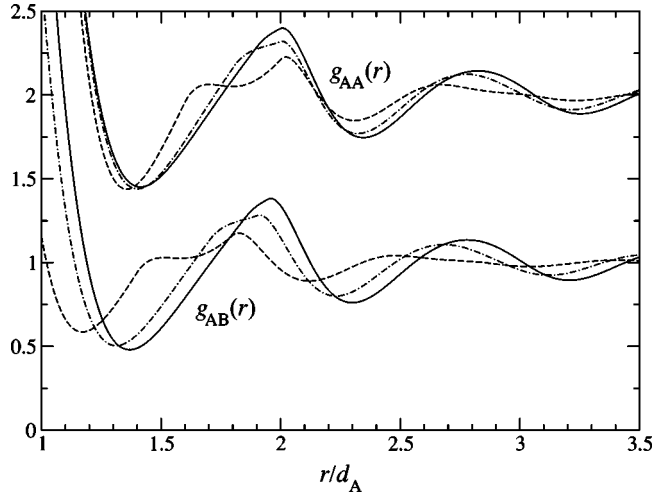

FIG. 4. Results within the Percus-Yevick approximation for the partial pair correlation functions $g_{AA}(r)$ and $g_{AB}(r)$ of binary HSM at $\varphi=0.516$; $\hat{x}_B=0.2$; and $\delta=0.9$ (solid lines), $\delta=0.8$ (dot-dashed lines), and $\delta=0.6$ (dashed lines). Curves for $g_{AA}(r)$ have been shifted up by 1.0 for clarity.

is provided by the partial pair distribution functions $g_{\alpha\beta}(r)$. These have been obtained by numerically solving the Ornstein-Zernike equation in the r domain using Baxter's factor function for the PY closure. The results are shown in Fig. 4 for $g_{AA}(r)$ and $g_{AB}(r)$, again at fixed φ and $\hat{x}_B$ for various δ. Here, both quantities vary more or less in phase for $\delta \gtrsim 0.7$, indicating that the local ordering of the one-component system is only slightly disturbed. One infers the B particles to be responsible for smaller average particle distances, thus favoring arrest of the structure. For smaller δ, the one-component system's structure is modified more severely, since $g_{AA}(r)$ and $g_{AB}(r)$ no longer vary in phase. Instead, ''chemical ordering'' effects can be seen, and they are responsible for the shift of the glass transition to higher packing fractions.

Let us stress that the variation of φ^c with concentration, while being small in total, nevertheless has a large impact on the dynamics close to the glass transition. This holds since relaxation times of the liquid in this region depend strongly on the distance to the critical packing fraction. We shall recur to this point in Sec. V A.

IV. GLASS FORM FACTORS

The spontaneous arrest of density fluctuations within the glass state is quantified by the glass form factors $F_{\alpha\beta}(q)$. In principle, these quantities can be measured in a scattering experiment via the intensity of the elastic line in the cross section. The diagonal elements $\hat{f}_{\alpha\alpha}(q)$ of the normalized quantities,

$$\hat{f}_{\alpha\beta}(q)=F_{\alpha\beta}(q)/\sqrt{S_{\alpha\alpha}(q)S_{\beta\beta}(q)}, \tag{10}$$

have the meaning of the Debye-Waller factor for the distribution of species α. In the limit $\hat{x}_B \to 0$, $\hat{f}_{BB}(q)$ is the spatial Fourier transform of the density distribution of a single localized B particle. It is the Lamb-Mößbauer factor $f_B^s(q)$ of a B particle in the hard-sphere system of A particles. A similar statement holds with the role of A and B particles interchanged, i.e., $f_A^s(q)=\hat{f}_{AA}(q,\hat{x}_B \to 1)$, but then the tagged particle is of the size $1/\delta$ in units of the diameter of the surrounding hard spheres'. If the packing fraction φ decreases towards the transition value φ^c, the $\hat{f}_{\alpha\alpha}(q)$ decrease towards their critical values, $\hat{f}_{\alpha\alpha}^c(q)$. These values are of particular relevance since they specify the so-called plateau values of the correlation functions of the liquid for states near the liquid-glass transition [42]. This will be discussed further in Sec. V.

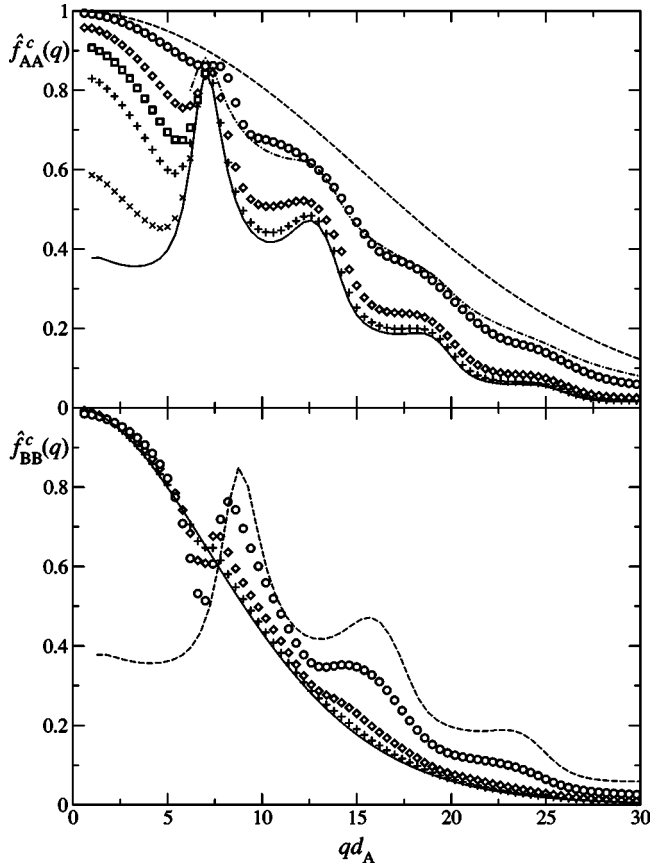

FIG. 5. Critical glass form factors $\hat{f}_{\alpha\alpha}^c(q)=F_{\alpha\alpha}^c(q)/S_{\alpha\alpha}(q)$ of a binary HSM with size ratio $\delta=0.8$ for the large (upper panel) and small (lower panel) particles. The packing contributions of the small spheres are $\hat{x}_B=0$ (solid lines), 0.05 (plus symbols), 0.2 (diamonds), 0.6 (circles), and 1.0 (dashed lines). In the upper panel, results for small q at $\hat{x}_B=0.01$ (crosses) and 0.1 (squares) are also shown. The dash-dotted line in the upper panel demonstrates the linear interpolation between the cases $\hat{x}_B=0$ and $\hat{x}_B=1$ for $qd_A \gtrsim 6$.

Figure 5 shows the critical Debye-Waller factors for small size disparity, $\delta=0.8$, and various $\hat{x}_B$. One notices an increase of the values with increasing $\hat{x}_B$ for almost all q. This result can be understood as follows. With no second species present, $\hat{f}_{AA}^c(q)$ matches the Debye-Waller factor of the one-component system, $f^c(q)$, shown by the full line in the upper

panel. On the other hand, as mentioned above, for $\hat{x}_B \to 1$, the quantity $\hat{f}^c_{AA}(q)$ crosses over to the tagged-particle quantity of a bigger sphere in a surrounding fluid of smaller ones, $f^{s,c}_A(q)$. At $q \to 0$ and $\hat{x}_B = 0$, momentum conservation implies $\hat{f}^c_{AA}(q \to 0) < 1$; while for $\hat{x}_B \to 1$, particle conservation and momentum relaxation for the tagged particle require $f^{s,c}_A(q \to 0) = 1$ [42]. By interpolation, one gets an increase in $\hat{f}^c_{AA}(q)$ with increasing $\hat{x}_B$ at small q. For large q, on the other hand, the Debye-Waller factor in a one-component system is oscillating around the Lamb-Mößbauer factor of a tagged particle with equal diameter. The Lamb-Mößbauer factor in turn can be approximated reasonably by a Gaussian $f^s(q) = \exp[-(qr_s)^2]$, where r_s is the particle's localization length [43]. The smaller the localization length becomes, the bigger the radius d^s of the tagged particle is with respect to the radius d of the surrounding spheres [43]; in particular, one gets for a tagged particle of diameter $d^s/d = 1/0.6$ (1/0.8, 0.8, 0.6) the value $r^c_s/d = 0.041$ (0.056, 0.095, 0.136). This implies the distribution of the $\hat{f}^c_{AA}(q)$, given in the limit $\hat{x}_B \to 1$ by $f^{s,c}(q)$ with $d^s/d = \delta$, to be broader than that in the limit $\hat{x}_B \to 0$, given by $f^c(q)$. Therefore the width of the distribution $\hat{f}^c_{AA}(q)$ has to increase for $\delta < 1$ as $\hat{x}_B$ increases from zero to unity. This is demonstrated in the upper panel by the dash-dotted line. It represents a simple interpolation, $\hat{f}^c_{AA}(q) \approx f^c(q) + [f^{s,c}_A(q) - f^c(q)]\hat{x}_B$ for $\hat{x}_B = 0.6$ and $q > 6/d_A$.

The change of $\hat{f}^c_{BB}(q)$ can be understood along the same line of reasoning. But one has to notice that in this case the localization length of a smaller sphere in a surrounding of big ones matters. In particular, one has $\hat{f}^c_{BB}(q, \hat{x}_B \to 0) = f^{s,c}_B(q/\delta)$. This yields a width of this distribution smaller than the one of the $\hat{f}^c_{BB}(q, \hat{x}_B \to 1) = f^c(q/\delta)$. Such an effect can be seen in the lower panel of Fig. 5 for $qd_A \gtrsim 7$. The crossover is naturally given by the size of the A particles. Based on the above argument, one expects at smaller q the inverse trend. But this is only found in $\hat{f}^c_{BB}(q)$ for $5 \lesssim qd_A \lesssim 7$. Instead one notices that for all $\hat{x}_B \leqslant 0.6$, the $\hat{f}^c_{BB}(q)$ follow closely the result for $\hat{x}_B = 0$, i.e., they are still close to unity at small q. This is a consequence of the normalization chosen here, since it is dominated by a change in $S_{BB}(q)$ at small q. It could be eliminated when discussing, e.g., matrix-normalized quantities, $\boldsymbol{f}(q) = \boldsymbol{S}^{-1/2}(q)\boldsymbol{F}(q)\boldsymbol{S}^{-1/2}(q)$, where the normalization properly accounts for the overall change in $\boldsymbol{S}(q)$.

The above argument only depends on the fact that $\delta < 1$, but not on the precise ratio of localization lengths. Thus it is quite general in binary HSM. Figure 6 shows the scenario for $\delta = 0.6$, i.e., for a larger size disparity, and indeed one recognizes the same trends as above. Here, the deviations of $\hat{f}^c_{BB}(q)$ from the tagged particle's $f^{s,c}_B(q)$ set in faster with increasing $\hat{x}_B$ than it was the case for $\delta = 0.8$. But one has to keep in mind that for smaller δ, the changes in $\hat{x}_B$ induce larger changes in the number concentration x_B, [cf. Eq. (8)]. The description of $\hat{f}^c_{AA}(q)$ as a simple interpolation between

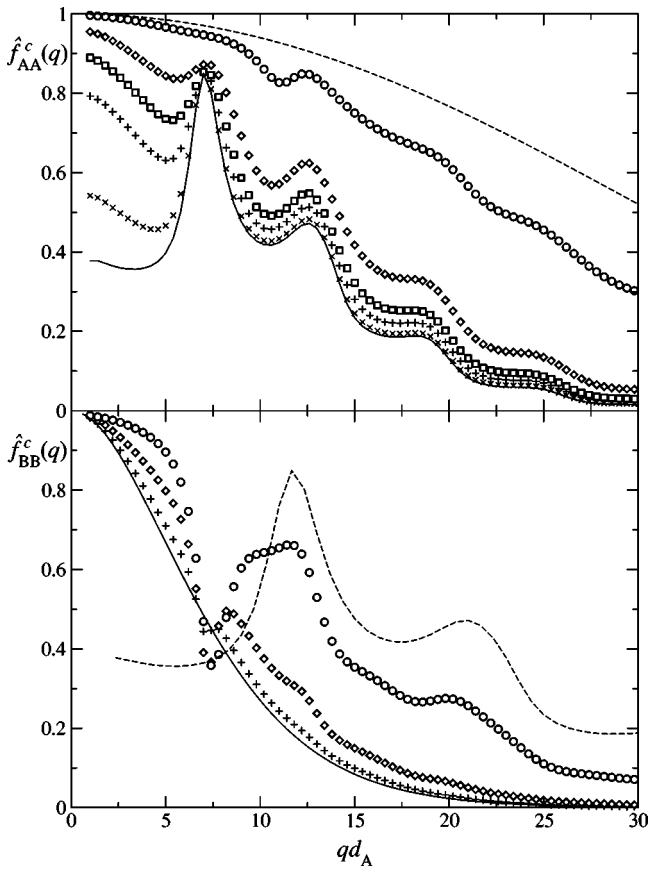

FIG. 6. Same as Fig. 5, but for size ratio $\delta = 0.6$.

$f^{s,c}_A(q)$ and $f^c(q)$ as explained above is notably worse, indicating that this simple picture quantitatively only works for δ not too different from unity. Also more pronounced in this case are the changes in $\hat{f}^c_{BB}(q)$ for small q, going back to the same reason as outlined above. Let us note in addition that for both δ, the trend noticed for the diagonal elements is also found for $\tilde{f}_{AB}(q) = F_{AB}(q)/S_{AB}(q)$, provided one is sufficiently far away from those q where a divergence due to vanishing $S_{AB}(q)$ occurs.

Macroscopic mechanic stability of the system is characterized by the elastic moduli. The liquid exhibits a longitudinal elastic modulus given by the structure factor through $M^0_L = \varrho(k_BT)\Sigma_{\alpha\beta}x_\alpha S^{-1}_{\alpha\beta}(q \to 0)x_\beta$ [44]. In the glass, the longitudinal modulus M_L is larger, $M_L = M^0_L + \delta M_L$, due to the arrest of the structure, [Eq. (5)]. Figure 7 shows the results for the binary HSM at the transition points for $\delta = 0.6$, 0.7, and 0.8 and also the critical shear modulus, [Eq. (6)]. All quantities are shown in units of (ϱk_BT) in order to more clearly reveal the effect of composition change. Note that the total density ϱ of the system increases and superimposes a rise in the moduli one could call an ''ideal mixing'' contribution. This ideal mixing value is given by the one-component values, $\delta M^c_L \approx 56.9$ and $M^c_T \approx 18.3$, shown through dashed lines in Fig. 7. At intermediate $\hat{x}_B$, strong deviations from ideal mixing occur. For all δ investigated here, the moduli decrease below their one-component values, indicating that the system becomes softer upon addition of

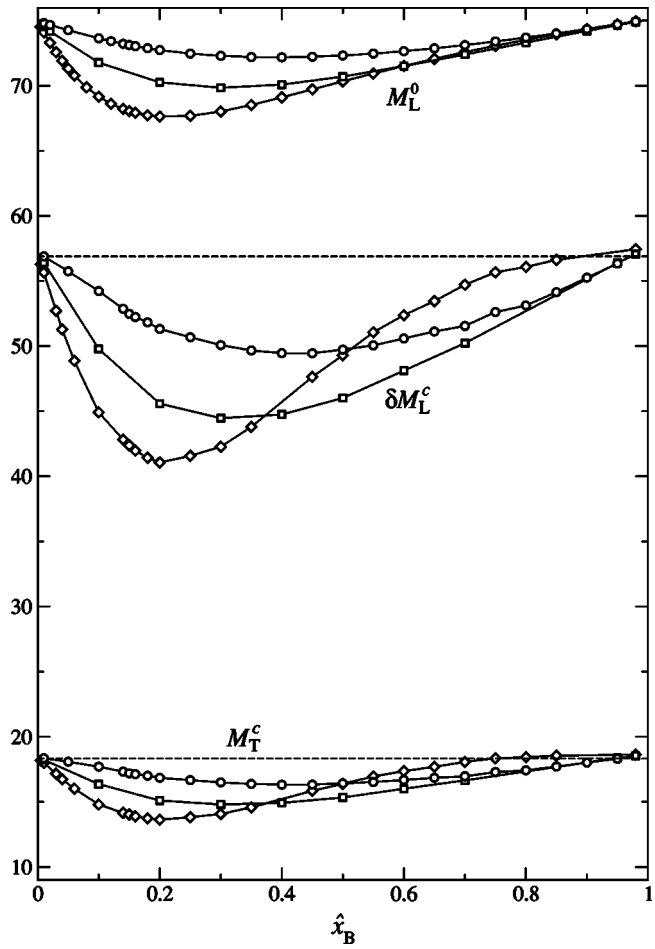

FIG. 7. Isothermal longitudinal elastic modulus M_L^0, increase of the longitudinal elastic modulus at the transition points δM_L^c, and transversal elastic modulus M_T^c at the liquid-glass transition points in units of $\varrho k_B T$ as functions of the packing contribution $\hat{x}_B$ of the smaller particles for size ratios $\delta=0.8$ (circles), 0.7 (squares), and 0.6 (diamonds). The dashed lines indicate the corresponding ideal mixing values evaluated for the one-component system.

smaller spheres. The effect increases with decreasing δ and it is of the order of 40% for $\delta=0.6$. It is partly connected with a corresponding increase in compressibility $\kappa=1/M_L^0$. Indeed, one observes for the given δ, minima in all three quantities at roughly the same $\hat{x}_B$. Let us nevertheless point out that apart from this thermodynamic contribution to the softening of the glass, mode-coupling effects still are necessary to explain the moduli for $\delta=0.6$. This can be inferred from the crossing of the M_T^c-versus $\hat{x}_B$ and δM_L^c-versus-$\hat{x}_B$ curves that is absent in M_L^0.

V. DYNAMICS

Close to an ideal glass transition, the essential aspects of the dynamics are described by a universal scenario. This scenario has been discussed comprehensively for one-component systems [35]. The results of Ref. [27] assure that these universal results are shared by the dynamics of the HSM. In particular, a two-step decay process arises, with plateau values given by the critical glass form factors $\hat{f}_{\alpha\beta}^c(q)$, and power-law relaxations towards and from the plateau, governed by anomalous exponents. If the total packing fraction is increased towards the critical value φ^c with other parameters kept fixed, a drastic increase in the relaxation time τ_α of the slowest decay process is obtained that is typical for glass-forming liquids.

In this section, we shall focus on the general, but nonuniversal features of the glassy relaxation in the binary HSM. To demonstrate the changes induced by different compositions, let us investigate a horizontal intersection of the transition diagram of Fig. 1 and consider a change of the composition $\hat{x}_B$ for the total packing fraction fixed at $\varphi=0.515$, i.e., at a value slightly below the glass transition of the one-component hard-sphere system. As above, the two different general scenarios, large and small size disparity, shall be demonstrated using the values $\delta=0.6$ and $\delta=0.8$, respectively.

A. General features

The dynamics for $\hat{x}_B \leqslant 0.2$ is demonstrated by Figs. 8 and 9 for the AA and BB correlation functions. We chose the wave vector $q=5.4/d_A$ below the peak in $\hat{f}_{AA}^c(q)$; it corresponds roughly to the one used in the light-scattering experiment of Ref. [1]. The normalized correlators $\hat{\phi}_{\alpha\alpha}(q,t)=\phi_{\alpha\alpha}(q,t)/S_{\alpha\alpha}(q)$ cross their plateau values $\hat{f}_{\alpha\alpha}^c(q)$ at certain times, say $t_\alpha(q)$, $\hat{\phi}_{\alpha\alpha}(q,t_\alpha(q))=\hat{f}_{\alpha\alpha}^c(q)$, which are marked by filled diamonds in the figures. Close to the transition, the correlators are close to this plateau for a large time interval. This is a manifestation of the cage effect. In a leading-order approximation for $\varphi^c-\varphi$ tending to zero, the time scale $t_\alpha(q)$ neither depends on α nor on q [42]. The independence of α is demonstrated to a good approximation in the figures. As explained in connection with Figs. 5 and 6, the plateau increases with increasing $\hat{x}_B$ and the increase is more pronounced for the larger majority particles A than for the smaller minority particles B.

The decay of the correlators below the plateau is referred to as the α process. A characteristic time scale $\tau_\alpha(q)$ for this process shall be defined by specifying 90% of the decay: $\hat{\phi}_{\alpha\alpha}(q,\tau_\alpha(q))=0.1\,\hat{f}_{\alpha\alpha}^c(q)$. These times are marked by open diamonds in the figures. For $\delta=0.8$, Fig. 8 demonstrates that the α-relaxation scale increases with increasing $\hat{x}_B$. This reflects the fact that with increasing $\hat{x}_B$ the state corresponds to a smaller distance from the transition point (compare Fig. 1).

The scenario for $\delta=0.6$, exhibited in Fig. 9, appears more subtle. In this case, the glass-transition diagram implies the distance to the transition to increase with increasing $\hat{x}_B$, thus leading to faster decay on the α time scale. But the effect of increasing plateau values with increasing $\hat{x}_B$ was seen above to occur for all δ. The combination of these effects leads to a crossing of correlators, as has also been observed in experiment [1].

In a dynamical light-scattering experiment, one does not measure the $\Phi_{\alpha\beta}(q,t)$ directly. Rather, one measures a sum

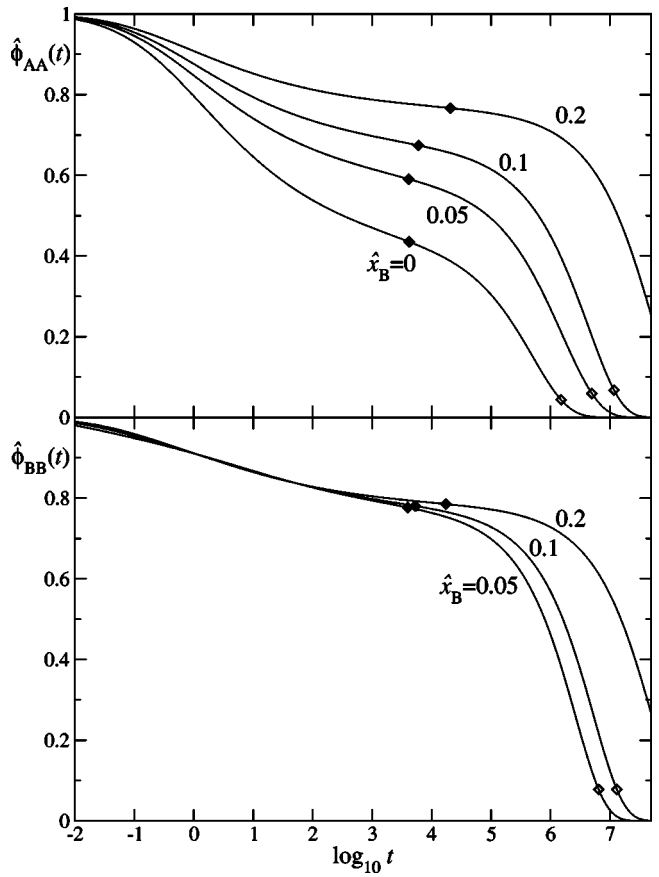

FIG. 8. Normalized partial density correlation functions $\hat{\phi}_{\alpha\alpha}(q,t)=\Phi_{\alpha\alpha}(q,t)/S_{\alpha\alpha}(q)$ for $\alpha=A$, B of a binary HSM with size ratio $\delta=0.8$ and different packing contributions of the smaller particles $\hat{x}_B$ for fixed packing fraction $\varphi=0.515$. The wave vector is $qd_A=5.4$. The unit of time here and in the following figures is chosen so that the short-time diffusivity is $D_\alpha^0=0.01/d_\alpha$. Filled diamonds mark the intersection of the decay curves with the plateau value $\hat{f}^c_{\alpha\alpha}(q)$. The open diamonds mark α-relaxation time scales $\tau_\alpha(q)$ defined by $\hat{\phi}_{\alpha\alpha}(q,\tau_\alpha(q))/\hat{f}^c_{\alpha\alpha}(q)=0.1$.

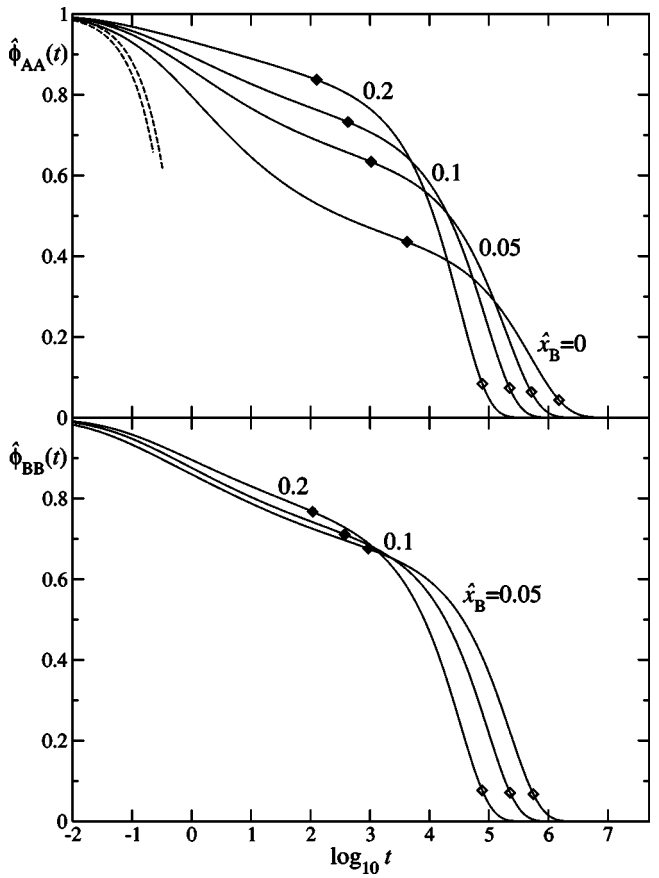

FIG. 9. Normalized partial density correlation functions $\hat{\phi}_{\alpha\alpha}(q,t)$ as in Fig. 8, but for the size ratio $\delta=0.6$. The dashed lines in the upper panel show the short-time approximation according to Eq. (14) for $\hat{x}_B=0$ and 0.2, from left to right.

weighted with the scattering amplitudes $b_\alpha(q)$ [45],

$$\phi^m(q,t)=\frac{1}{\mathcal{N}_q}\sum_{\alpha\beta} b_\alpha(q)b_\beta(q)\Phi_{\alpha\beta}(q,t). \qquad (11)$$

Here, $\mathcal{N}_q$ is some normalization constant chosen to satisfy $\phi^m(q,t=0)=1$. It was a crucial point in Ref. [1] to be able to vary the $b_\alpha(q)$ without altering the dynamics. Thus, three independent measurements of $\phi^m(q,t)$ could be used to invert Eq. (11) and therefore to determine the three distinct functions $\Phi_{\alpha\beta}(q,t)$. The latter are better suited for a comparison with the theory. But let us also demonstrate the dynamics for a typical example of the directly measured function $\phi^m(q,t)$. If one assumes the colloidal particles to be uniform spheres, one gets [45]

$$b_\alpha(q)\propto\frac{d_\alpha^3}{(qd_\alpha)^3}\left(\sin(qd_\alpha/2)-\frac{qd_\alpha}{2}\cos(qd_\alpha/2)\right). \qquad (12)$$

Figure 10 shows the results for $\delta=0.6$ and $\delta=0.8$ at $qd_A=5.4$. The same qualitative picture as discussed above for the $\hat{\phi}_{AA}(q,t)$ correlator arises, yet the increase in plateau values is less pronounced. The reason is a destructive interference effect in Eq. (11) caused by $\Phi_{AB}(q,t)\leqslant 0$. This holds especially for $\delta=0.8$, and also for smaller wave vectors. Nonetheless, some increase remains in all cases, and one should be able to see this in experiment. One could be tempted to analyze such data in terms of a one-component model. However, this would be misleading. For a one component system, the observed increase of the plateau $f^{m,c}(q)=\Sigma_{\alpha\beta}b_\alpha(q)b_\beta(q)F^c_{\alpha\beta}(q)$ would imply that the system becomes stiffer upon increasing the contribution of smaller particles. But we have seen above from a discussion of the mechanical moduli that the opposite is the case.

Figure 11 exhibits α-relaxation scales τ_A for the larger particles as a function of mixing. It corroborates the picture suggested by the glass-transition diagram. Since the α relaxation close to the glass transition varies as $\tau_\alpha\sim(\varphi^c-\varphi)^{-\gamma}$, $\gamma>2.5$, the variations of τ_A are much more pronounced than those of φ^c. Note that the values of τ_A for different δ do not necessarily coincide at $\hat{x}_B=1$. MCT predicts all α-relaxation times $\tau_\alpha(q)$ to be coupled. Thus, the qualitative picture demonstrated in Fig. 11 will also hold for the α-relaxation scales

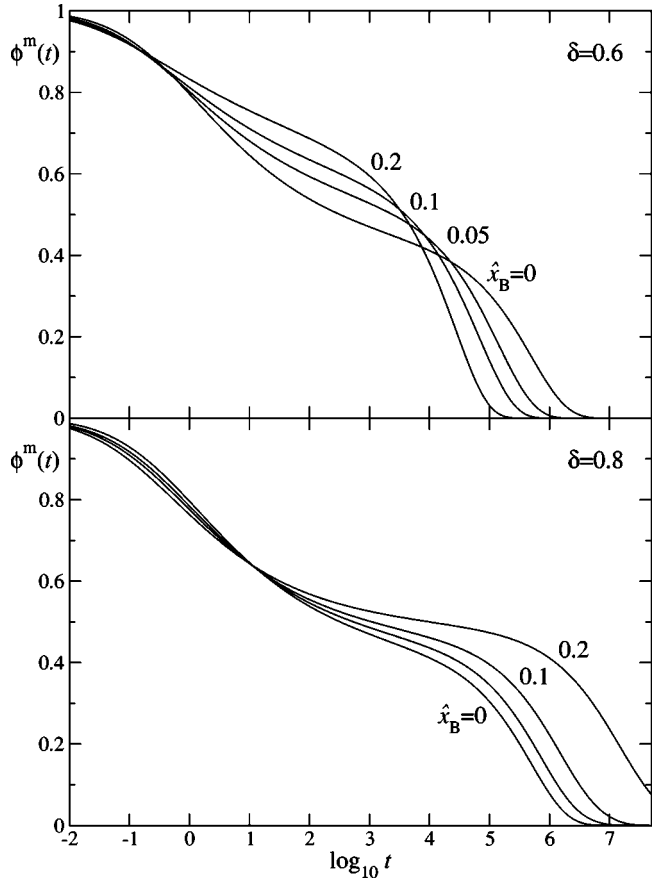

FIG. 10. Sum $\phi^m(q,t)$ of the partial density correlation functions $\Phi_{\alpha\beta}(q,t)$ at wave vector $qd_A=5.4$, weighted according to Eq. (11) with scattering amplitudes $b_\alpha(q)$ as specified in Eq. (12). The packing fraction is kept constant at $\varphi=0.515$, and $\hat{x}_B=0$, 0.05, 0.1, 0.2 as indicated by the labels. The upper panel shows the results for size ratio $\delta=0.6$, the lower one for $\delta=0.8$.

of other experimental quantities such as the viscosities or inverse diffusivities. Nucleation rates are also affected by the diffusivities; thus Fig. 11 demonstrates a possible reason for nucleation in binary mixtures to vary strongly with changes of the composition.

B. Dynamics close to the plateau

One notices in Figs. 8 and 9 a trend for the relaxation onto the plateau value. This part of the curve, which deals with the onset of structural relaxation, displays a slowing down of the relaxation with increasing $\hat{x}_B$ for both cases considered for δ. In principle, the relaxation in this time window is a result of both structural and transient relaxation. In a leading approximation, the latter is given by

$$\mathbf{\Phi}(q,t)=\exp[-q^2\boldsymbol{D}(q)t]\boldsymbol{S}(q), \tag{13}$$

with the matrix $\boldsymbol{D}(q)$ of short-time collective diffusion constants, $\boldsymbol{D}(q)=(q^2\boldsymbol{\tau}(q))^{-1}\boldsymbol{S}(q)^{-1}$. In particular, for a binary mixture this yields

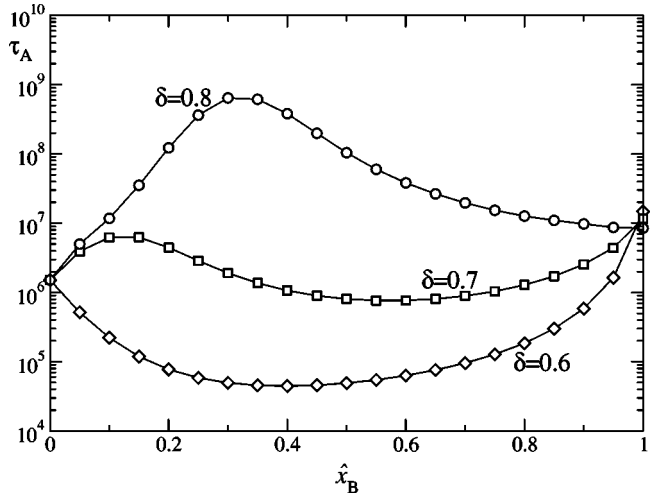

FIG. 11. α time scale τ_A defined through $\hat{\phi}_{AA}(q,\tau_A)=0.1\,\hat{f}^c_{AA}(q)$ for $qd_A=5.4$ at packing fraction $\varphi=0.515$, and $\delta=0.8$ (circles), 0.7 (squares), and 0.6 (diamonds). The lines are guides to the eye.

$$\hat{\phi}_{AA}(q,t)=1-q^2D'(q)t+\mathcal{O}(t^2), \tag{14}$$

where $D'(q)=x(q)D(q)$ with $x(q)=S(q)/S_{AA}(q)$, and $D(q)$ and $S(q)$ are the diffusion constant and the structure factor of the one-component system, respectively. It has already been noticed in Ref. [1] that $x(q)<1$ for small q. Thus, one expects a slowing down of the short-time diffusion due to mixing in the limit of small q. For the wave vector discussed here, however, the effect is small: with $\delta=0.6$, $\varphi=0.515$, and $qd_A=5.4$, one gets $x\approx0.82$ (0.76,0.78) for $\hat{x}_B=0.05$ (0.1, 0.2). The approximations resulting from Eq. (14) are shown for $\hat{x}_B=0$ and 0.2 as dashed lines in Fig. 9. One infers that this describes the dynamics only for $\hat{\phi}_{AA}(q,t)\geqslant0.98$. Note that $x(q)$ is not monotonous in $\hat{x}_B$, but the mentioned increase in the stretching of the short-time relaxation with increasing $\hat{x}_B$ is. Furthermore, at still larger wave vectors, one has $x(q)>1$ as $x(q\to\infty)=1/x_A$, yielding faster short-time diffusion in the mixture. But the slowing down of the relaxation towards the plateau persists also for large q, as can be inferred from the numerical solutions. Thus we conclude that the change in the short-time diffusion coefficients is not sufficient to explain the observed effect.

Let us now focus on the structural relaxation as defined in Sec. II A. Figure 12 presents solutions of Eqs. (3) for $\delta=0.6$ and different $\hat{x}_B$ at fixed φ, together with the solutions reproduced from Fig. 9. The long-time parts of corresponding curves can be scaled on top of each other, since there the dynamics depends on the short-time behavior only through a scaling time t_0, as is demonstrated for the $\hat{x}_B=0.2$ curve. For other $\hat{x}_B$, the same observation is valid. Nevertheless, we have applied the same rescaling as used for $\hat{x}_B=0.2$ instead of matching t_0 and t_* independently for different $\hat{x}_B$. This is done in order to also demonstrate the drift of the scaling time $t_0(\hat{x}_B)$ with $\hat{x}_B$. At short times, all structural relaxation

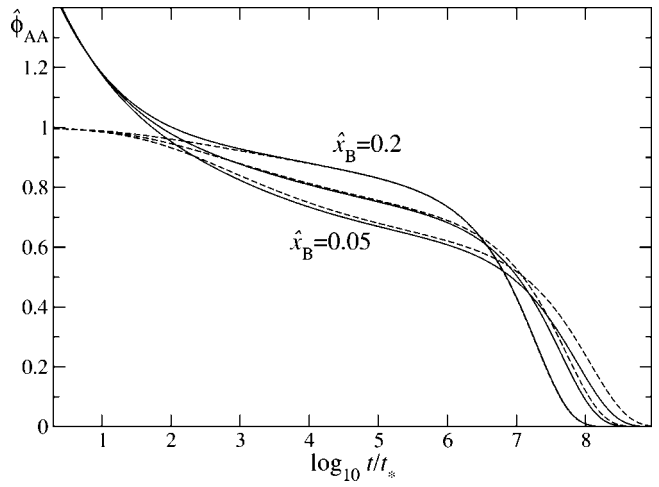

FIG. 12. Structural relaxation dynamics (solid lines) as defined by Eqs. (3) for a binary HSM with $\delta=0.6$ and $\varphi=0.515$, with small particle packing contributions $\hat{x}_B=0.2$, 0.1, and 0.05 as indicated. The dashed lines are the solutions for the same parameters of the general MCT equations, [Eqs. (1)], with the time scaled to match the structural-relaxation solution at long times for $\hat{x}_B=0.2$.

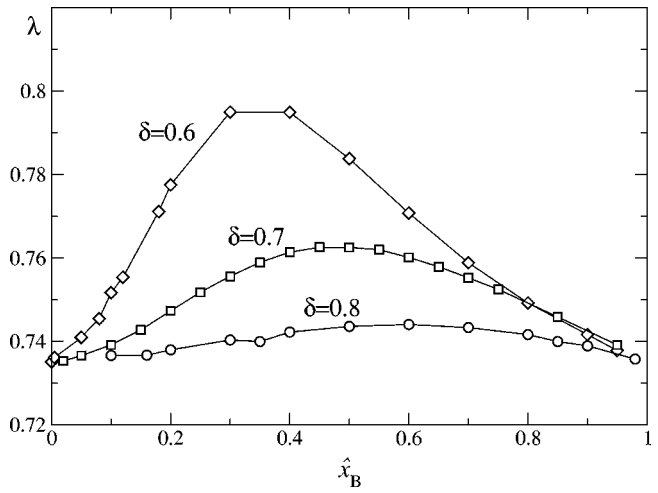

FIG. 13. Exponent parameters λ corresponding to the points shown in the transition diagram, Fig. 1; symbols indicate $\delta=0.6$ (diamonds), 0.7 (squares), and 0.8 (circles). The lines are guides to the eye.

curves follow the same asymptote $t^{-1/3}$, and one notices that they deviate from one another at roughly $t=10\,t_*$. This demonstrates that the increase of the stretching in the initial decay with increasing $\hat{x}_B$, exhibited for $2.5\lesssim\log_{10}(t/t_*)\lesssim5.5$, is a result of structural relaxation rather than transient dynamics.

In order to achieve a deeper understanding of the conclusions concerning the initial part of the structural relaxation processes demonstrated above, recall that one can derive scaling laws for an analytical description of the correlators near their plateau values. This has been discussed comprehensively for the one-component system in Ref. [35]. The theory is based on the observation that the liquid-glass transition is described by an A_2 bifurcation of Eq. (2a) for the glass form factors. It is straightforward to generalize the theory for one-component systems to the case of interest here [46]. Let us merely note the basic results necessary to understand the following figures.

For the asymptotic expansion, one identifies a small parameter σ and, connected to it, a time scale $t_\sigma=t_0|\sigma|^{-1/(2a)}$. Here, the critical exponent $0<a<1/2$ is one of the nontrivial exponents of MCT that is calculated from the mode-coupling functional at the transition via the so-called exponent parameter $\lambda[\lambda=\Gamma(1-a)^2/\Gamma(1-2a)]$. The separation parameter σ is also calculated from the mode-coupling functional, and is a smooth function of the control parameters that vanishes at the transition. The conditions $\sigma>0$ and $\sigma<0$ characterize glass states and liquid states, respectively. Setting $\hat{t}=t/t_\sigma$, one obtains an expansion in the small quantity $\sqrt{|\sigma|}$,

$$\begin{aligned}\mathbf{\Phi}(q,t)-\boldsymbol{F}^c(q)=&\boldsymbol{H}(q)\sqrt{|\sigma|}g(\hat{t})+\boldsymbol{H}(q)[|\sigma|h(\hat{t})+\sigma\nu]\\&+\boldsymbol{K}(q)[|\sigma|g(\hat{t})^2-\sigma/(1-\lambda)]\\&+\overline{\boldsymbol{K}}(q)\sigma/(1-\lambda)+\mathcal{O}(|\sigma|^{3/2}).\end{aligned}\tag{15}$$

Let us first explain the leading-order contribution, that is given by the first line of Eq. (15). It demonstrates the so-called factorization theorem, in that it splits the wave-vector and control-parameter dependence off from the time dependence. It is the critical eigenvector $\boldsymbol{H}(q)$ introduced above that governs the former. The latter is given by a master function $g(\hat{t})$ that is the solution of

$$\frac{d}{d\hat{t}}\int_0^{\hat{t}}g(\hat{t}-t')g(t')dt'=\lambda g(\hat{t})^2+\mathrm{sgn}\,\sigma,\tag{16}$$

obeying $g(\hat{t}\to0)\sim(t/t_0)^{-a}$. The shape function $g(\hat{t})$ does not depend on the details of the mode-coupling vertices, but only on the exponent parameter λ. Thus, the factorization theorem predicts that all correlators for all models resulting in the same λ can be rescaled to have the same shape, given by the master function $g(\hat{t})$.

The corrections to the specified scaling law are given by the terms of order σ in Eq. (15). They consist of a part parallel to the critical amplitude $\boldsymbol{H}(q)$, where a new correction-to-scaling shape function $h(\hat{t})$ and a constant determined by the details of the mode-coupling vertices ν appear. In addition, two correction amplitudes $\boldsymbol{K}(q)$ and $\overline{\boldsymbol{K}}(q)$ to be evaluated from the mode-coupling functional, are introduced by the next-to-leading order. They explain that factorization holds with different quality for different correlators. One finds the $K_{AA}(q)$ and $\overline{K}_{AA}(q)$ to show the same qualitative variation with q in the HSM considered here as in the one-component case discussed in Ref. [35]. The only parameter that cannot be calculated within this approach is the time scale t_0; it is fixed by matching the long-time limit of the asymptotic solution at the critical point, $\mathbf{\Phi}^c(q,t)=\boldsymbol{F}^c(q)+\boldsymbol{H}(q)(t/t_0)^{-a}+\mathcal{O}(t^{-2a})$, to the numerical solution at long times.

We first investigate the variation of λ as a function of the composition, shown in Fig. 13. The exponent parameter is

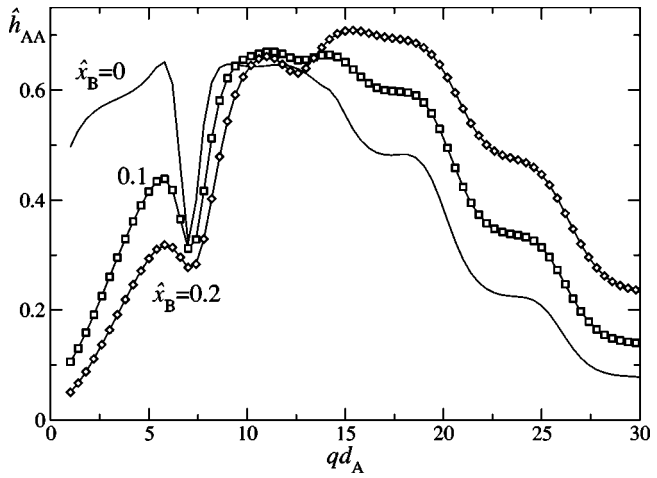

FIG. 14. Normalized critical amplitudes $\hat{h}_{AA}(q) = H_{AA}(q)/S_{AA}(q)$ for $\delta = 0.6$ and $\hat{x}_B = 0.0$, 0.1, and 0.2 as indicated.

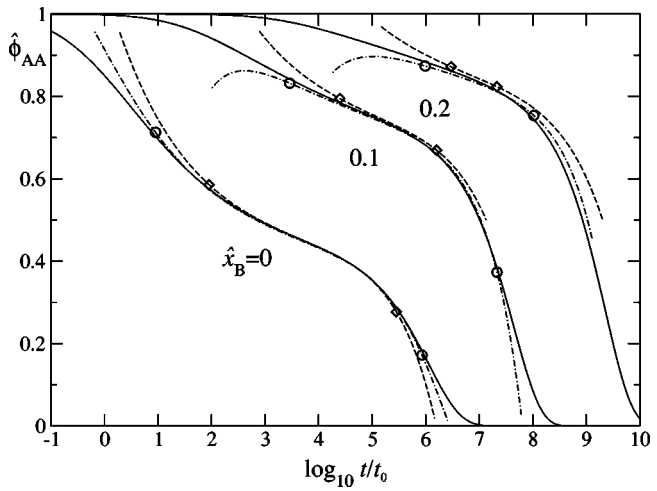

FIG. 15. Asymptotic description of the normalized correlation functions $\hat{\phi}_{AA}(q,t)$ for $qd_A = 5.4$, $\varphi = 0.515$, $\delta = 0.6$ and different $\hat{x}_B$ as indicated. The solid lines are the full solutions reproduced from Fig. 9, but plotted as functions of t/t_0. The time scale t_0 is 0.4408, 0.2026, and 0.1385 for $\hat{x}_B = 0$, 0.1, and 0.2, respectively. Dashed and dash-dotted lines show the results of Eq. (15) up to order $|\sigma|^{1/2}$ and $|\sigma|$, respectively. The diamonds (circles) mark where the asymptotic solution up to leading (next-to-leading) order deviates by 0.01 from the normalized correlator. Curves for $\hat{x}_B = 0.1$ (0.2) have been translated along the t axis by 2 (4) decades for clarity.

larger than the value found for the pure hard-sphere system, $\lambda(\hat{x}_B = 0) = \lambda(\hat{x}_B = 1) = 0.736$. It exhibits a maximum smaller than 0.8 for $\delta \geqslant 0.6$. As a result, the critical exponent decreases relative to the value $a = 0.311$ for the hard-sphere system. In particular we get $\lambda = 0.752$ (0.778), and from this $a = 0.304$ (0.291) for $\hat{x}_B = 0.1$ (0.2). As a consequence, the stretching of the decay towards the plateau increases somewhat with increasing $\hat{x}_B$ and decreasing δ. But this effect is rather small and cannot explain the slowing down effect specified above.

Figure 14 shows the critical amplitudes $\boldsymbol{H}(q)$ in the case $\delta = 0.6$ for the AA correlator. The normalized quantity $\hat{h}_{AA}(q) = H_{AA}(q)/S^c_{AA}(q)$ was chosen to match the representation of Figs. 8 and 9. While there is no general trend valid for all q, we note that at the wave vector $q = 5.4/d_A$ shown above, $\hat{h}_{AA}(q)$ decreases significantly upon increasing $\hat{x}_B$. Let us emphasize that the region of $qd_A \lesssim 10$ is the one accessible in dynamical light-scattering experiments on colloidal systems. Furthermore, let us add that qualitatively the same change with $\hat{x}_B$, although less pronounced, is observed in the $\delta = 0.8$ case. The decrease of $\hat{h}_{AA}$ yields a flattening of the $\hat{\phi}(t)$-versus-log t curve within the time window that can be described by the leading-order contribution to Eq. (15). The identified effect is further increased since the time scale t_0 decreases with increasing $\hat{x}_B$. One gets $t_0 = 0.4408$ (0.2026, 0.1385) for $\hat{x}_B = 0$ (0.1, 0.2) and other microscopic parameters as given above.

Let us turn the preceding discussion into a quantitative demonstration by comparing in Fig. 15 the asymptotic formula with the complete solution for the $\hat{\phi}_{AA}$ correlator. The case $\hat{x}_B = 0$ shows a typical scenario for the one-component system, where the $\sqrt{|\sigma|}$ term of Eq. (15) describes over three decades in time of the solution, as indicated by the open diamonds. This window of the analytic description is expanded by the next-to-leading-order formula by about 1 decade both at short and at long times, as can be seen from the circle symbols. For $\hat{x}_B = 0.1$ and 0.2, the range of validity for both the leading and the next-to-leading order is seen to shrink; at $\hat{x}_B = 0.2$ it is, including corrections, only about 2 decades. But to understand this, one has to keep in mind that the distance from the critical point has increased by changing from $\hat{x}_B = 0$ to $\hat{x}_B = 0.2$ for fixed total packing. Indeed, we get $\sigma = -0.0027$ (-0.0066, -0.011) for $\hat{x}_B = 0$ (0.1, 0.2), i.e., an increase in σ by about a factor of 4. Thus, the de-

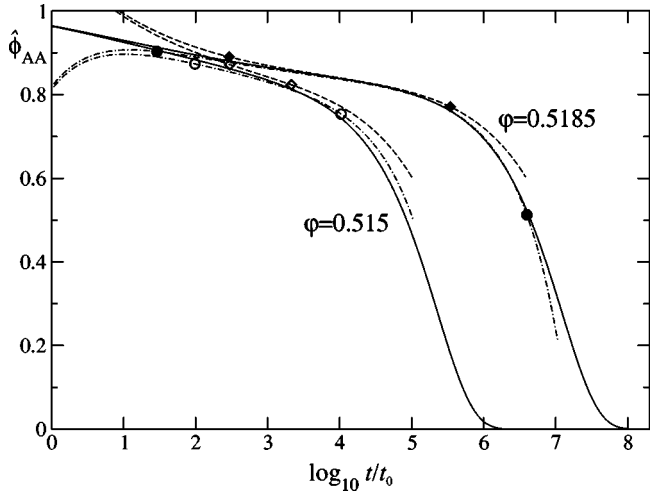

FIG. 16. Asymptotic description of the normalized correlation functions $\hat{\phi}_{AA}(q,t)$ for $qd_A = 5.4$, $\delta = 0.6$ and $\hat{x}_B = 0.2$ at different φ as indicated. Lines and symbols as in Fig. 15; open symbols refer to $\varphi = 0.515$ and closed ones to $\varphi = 0.5185$.

creasing quality of the asymptotic description is merely due to an increase of σ. This is corroborated by Fig. 16, where the $\hat{x}_B=0.2$ case is repeated together with a point closer to the transition. For $\hat{x}_B=0.2$ and $\varphi=0.5185$, the separation parameter is $\sigma=-0.0028$, similar to the value discussed in Fig. 15 for $\hat{x}_B=0$. Therefore, the regions of validity of the asymptotic expansions are similar as well. Indeed, the relevant quantity specifying the range of validity of the asymptotic expansion is not the size of the logarithmic time interval, but the size of the decay interval $|\hat{\phi}_{AA}(q,t)-\hat{f}^c_{AA}(q)|$. Figures 15 and 16 demonstrate that the analytic formula, [Eq. (15)] describes the structural relaxation in $\hat{\phi}_{AA}(q,t)$ towards the plateau $\hat{f}^c_{AA}(q)$ below 0.70, 0.85, and 0.90 for $\hat{x}_B=0$, 0.1, and 0.2, respectively. This is the regime where Fig. 9 exemplifies the slowing down of this decay with increasing $\hat{x}_B$ that was reported in Ref. [1].

VI. CONCLUSIONS

Within the mode-coupling theory (MCT) for a binary hard-sphere mixture, four mixing effects have been identified for states near the ideal liquid-glass transition. First, mixing suppresses intermediate-ranged ordering effects and this leads to an increase of the small wave-vector limit of the total structure factor, (Fig. 3). Equivalently, the compression modulus of the liquid decreases. A similar softening of the elastic restoring forces is found for the moduli for compression and shear of the glass near the transition points, (Fig. 7). Second, an apparently opposite phenomenon is exhibited by the increase of the Debye-Waller factors, i.e., a stiffening of the glass with respect to spontaneous density fluctuations, (Figs. 5 and 6). This means primarily that mixing for fixed packing leads to better localization of the particles. The third effect is closely related to this, viz., a stiffening of the cages of the localized particles upon changes of composition. These changes are described by the critical amplitude, that decreases upon mixing, as shown in Fig. 14. The universal MCT formula for the initial part of the structural relaxation, [Eq. (15)], shows that this leads to a slowing down of the short-time part of the glassy dynamics, as demonstrated in Figs. 8 and 9 and discussed quantitatively in Figs. 15 and 16. The above described second and third mixing effects have been identified originally in experiments on colloids [1].

The fourth general effect concerns the scale for the long-time relaxation, i.e., the scale for hydrodynamic phenomena such as diffusion, or, more generally, for the α-relaxation processes of the liquid. Two scenarios are found as exhibited by the liquid-glass transition diagram, by Fig. 1, or by Fig. 11. For small size disparity, mixing stabilizes the glass state. As described above for the initial part of the structural relaxation, also the final part of the decay is slowed down upon mixing. This is shown in Fig. 8 for the size ratio $\delta=0.8$. However, for larger size disparities, an entropically induced plasticizing effect is found. Due to mixing, the glass state is destabilized and the α-relaxation times decrease. As a result, the $\hat{\phi}(t)$-versus-log(t) diagrams cross upon mixing as shown in Fig. 9 and observed for $\delta=0.6$ in the experiments of Ref. [1].

In summary, our work demonstrates that MCT can explain qualitatively the mixing effects on the glassy dynamics of colloids observed for the size ratio $\delta=0.6$. A quantitative comparison of the results of our theory with the data of Ref. [1] will be discussed in a subsequent publication. Our theory suggests to also carry out experiments for a size ratio near $\delta=0.8$ since a different scenario is predicted for that case.

It can be expected that the results of our theory will also be of some relevance to experiments on glass-forming binary metal alloys. The formation of metallic glasses can to some extent be understood by treating the constituent atoms as hard spheres, which will then be all of similar size [47]. Even though in this paper we have dealt only with Brownian short-time dynamics relevant for colloidal suspensions, it is known that the long-time phenomena connected with the glass transition are the same for Newtonian dynamics [28,29]. Recently, the concentration dependence of the critical temperature T_c was discussed for a computer simulation of a $Co_{100-x}Zr_x$ model [48]. This simulation used fine-tuned pair potentials to model the metallic glass former; but if one estimates the size ratio of a corresponding hard-sphere mixture from the atomic radii of Co and Zr [49], one gets $\delta\approx 0.78$. Indeed, in the simulation the curve $T_c(x)$ was found to have a maximum at intermediate x, i.e., the glass transition was found to occur at smaller coupling strengths. But this corresponds to a decrease of φ^c in the HSM model. A similar reasoning holds for computer-simulated Ni-Zr melts [13].

Let us add some remarks on the results derived by Harbola and Das [24]. Their equations, as opposed to the ones studied in this paper, predict for the glass form factors $\hat{f}_{\alpha\beta}(q)$ and for the critical packing fraction of the glass transition φ^c, a dependence on the mass ratio m_A/m_B of the two species. This result appears surprising because one should not expect the equilibrium results for a classical system to depend on the particles' inertia parameters. It is obvious that the limit of vanishing concentration x_B has to reproduce the bell-shaped Lamb-Mößbauer factor for the glass form factor of the minority species, as discussed above in connection with Fig. 5. This result is not obtained in the theory of Ref. [24], which, as a consequence, does not reproduce the experimental finding of an increase in the correlator's plateau values upon mixing [1]. Furthermore, the theory of Ref. [24] predicts a much larger increase of the critical packing fraction φ^c upon mixing than measured [1]. Indeed, it predicts that the glass transition can disappear completely if the size ratio δ is smaller than a critical value. This result seems implausible, since there is no obvious mechanism that prevents the large particles from becoming a glass upon increasing the density.

ACKNOWLEDGMENTS

We thank W. van Megen, M. Sperl, and S. R. Williams for discussions and valuable comments on our manuscript. This work was supported by the Deutsche Forschungsgemeinschaft, through DFG Grant No. 154/12-1.

[1] S.R. Williams and W. van Megen, Phys. Rev. E **64**, 041502 (2001).
[2] W. van Megen and S.M. Underwood, Phys. Rev. E **47**, 248 (1993).
[3] W. van Megen, Transp. Theory Stat. Phys. **24**, 1017 (1995).
[4] W. Götze, J. Phys.: Condens. Matter **11**, A1 (1999).
[5] W. Kob, J. Phys.: Condens. Matter **11**, R85 (1999).
[6] W. Götze, A.P. Singh, and T. Voigtmann, Phys. Rev. E **61**, 6934 (2000).
[7] S.-H. Chong, W. Götze, and A.P. Singh, Phys. Rev. E **63**, 011206 (2001).
[8] W. Götze, in *Amorphous and Liquid Materials*, Vol. 118 of *NATO Advanced Study Institute, Series E: Applied Sciences*, edited by E. Lüscher, G. Fritsch, and G. Jacucci (Nijhoff, Dordrecht, 1987), pp. 34–81.
[9] J.-L. Barrat and A. Latz, J. Phys.: Condens. Matter **2**, 4289 (1990).
[10] M. Nauroth and W. Kob, Phys. Rev. E **55**, 657 (1997).
[11] W. Kob, M. Nauroth, and F. Sciortino, J. Non-Cryst. Solids **307–310**, 181 (2002).
[12] F. Sciortino and W. Kob, Phys. Rev. Lett. **86**, 648 (2001).
[13] A.B. Mutiara and H. Teichler, Phys. Rev. E **64**, 046133 (2001).
[14] J. Bosse and J.S. Thakur, Phys. Rev. Lett. **59**, 998 (1987).
[15] J.S. Thakur and J. Bosse, Phys. Rev. A **43**, 4378 (1991).
[16] J.S. Thakur and J. Bosse, Phys. Rev. A **43**, 4388 (1991).
[17] J. Bosse and Y. Kaneko, Phys. Rev. Lett. **74**, 4023 (1995).
[18] J. Bosse and Y. Kaneko, Prog. Theor. Phys. Suppl. **126**, 13 (1997).
[19] J.S. Thakur and J. Bosse, J. Non-Cryst. Solids **117/118**, 898 (1990).
[20] J. Bosse and S.D. Wilke, Phys. Rev. Lett. **80**, 1260 (1998).
[21] H.C. Chen, S.D. Wilke, and J. Bosse, Phys. Rev. B **60**, 12 045 (1999).
[22] G. Srinivas, A. Mukherjee, and B. Bagchi, J. Chem. Phys. **114**, 6220 (2001).
[23] A. Mukherjee, G. Srinivas, and B. Bagchi, Phys. Rev. Lett. **86**, 5926 (2001).
[24] U. Harbola and S.P. Das, Phys. Rev. E **65**, 036138 (2002).
[25] G. Nägele, Phys. Rep. **272**, 215 (1996).
[26] V.I. Arnol'd, *Catastrophe Theory*, 3rd ed. (Springer, Berlin, 1992).
[27] T. Franosch and T. Voigtmann, J. Stat. Phys. **109**, 237 (2002).
[28] T. Franosch, W. Götze, M.R. Mayr, and A.P. Singh, J. Non-Cryst. Solids **235-237**, 71 (1998).
[29] M. Fuchs and T. Voigtmann, Philos. Mag. B **79**, 1799 (1999).
[30] I.M. Mryglod, Condens. Matter Phys. **10**, 115 (1997).
[31] G. Nägele and J. Bergenholtz, J. Chem. Phys. **108**, 9893 (1998).
[32] J.L. Lebowitz and J.S. Rowlinson, J. Chem. Phys. **41**, 133 (1964).
[33] R.J. Baxter, J. Chem. Phys. **52**, 4559 (1970).
[34] A. Malijevský, M. Barošová, and W.R. Smith, Mol. Phys. **91**, 65 (1997).
[35] T. Franosch, M. Fuchs, W. Götze, M.R. Mayr, and A.P. Singh, Phys. Rev. E **55**, 7153 (1997).
[36] W. Götze, J. Stat. Phys. **83**, 1183 (1996).
[37] S. Asakura and F. Oosawa, J. Polym. Sci. **33**, 183 (1958).
[38] L. Fabbian, W. Götze, F. Sciortino, P. Tartaglia, and F. Thiery, Phys. Rev. E **59**, R1347 (1999).
[39] J. Bergenholtz and M. Fuchs, Phys. Rev. E **59**, 5706 (1999).
[40] K. Dawson, G. Foffi, M. Fuchs, W. Götze, F. Sciortino, M. Sperl, P. Tartaglia, T. Voigtmann, and E. Zaccarelli, Phys. Rev. E **63**, 011401 (2001).
[41] C. Lemaignan, Acta Metall. **28**, 1657 (1980).
[42] W. Götze, in *Liquids, Freezing and Glass Transition*, Proceedings of Les Houches Summer School of Theoretical Physics, Session LI, 1989, edited by J.P. Hansen, D. Levesque, and J. Zinn-Justin (North Holland, Amsterdam, 1991), pp. 287–503.
[43] M. Fuchs, W. Götze, and M.R. Mayr, Phys. Rev. E **58**, 3384 (1998).
[44] J.-P. Hansen and I.R. McDonald, *Theory of Simple Liquids*, 2nd ed. (Academic Press, London, 1986).
[45] P.N. Pusey, in *Liquids, Freezing and Glass Transition* (Ref. [42]), pp. 765–942.
[46] Th. Voigtmann, Ph.D. thesis, TU München, 2002.
[47] A. Meyer, e-print cond-mat/0206364.
[48] U.K. Rößler and H. Teichler, Phys. Rev. E **61**, 394 (2000).
[49] W. Paszkowicz, J. Phys. F: Met. Phys. **18**, 1761 (1988).